Journal of Applied Physics

RESEARCH ARTICLE | FEBRUARY 14 2022

Non-equilibrium spin noise spectroscopy of a single quantum dot operating at fiber telecommunication wavelengths

Tian-Jiao Sun; P. Sterin; L. Lengert; ... et. al

Journal of Applied Physics 131, 065703 (2022)
https://doi.org/10.1063/5.0078910

AIP Publishing

Journal of Applied Physics ARTICLE scitation.org/journal/jap

Non-equilibrium spin noise spectroscopy of a single quantum dot operating at fiber telecommunication wavelengths

Cite as: J. Appl. Phys. **131**, 065703 (2022); doi: 10.1063/5.0078910
Submitted: 16 November 2021 · Accepted: 23 January 2022 ·
Published Online: 14 February 2022

Tian-Jiao Sun,[1,2,3] P. Sterin,[1] L. Lengert,[1] C. Nawrath,[4] M. Jetter,[4] P. Michler,[4] Yang Ji,[2,3] J. Hübner,[1,a)] and M. Oestreich[1,b)]

AFFILIATIONS

[1]Institut für Festkörperphysik, Leibniz Universität Hannover, Appelstraße 2, D-30167 Hannover, Germany
[2]SKLSM, Institute of Semiconductors, Chinese Academy of Sciences, Beijing 100083, People's Republic of China
[3]Center of Materials Science and Optoelectronics Engineering, University of Chinese Academy of Sciences, Beijing 100049, People's Republic of China
[4]Institut für Halbleiteroptik und Funktionelle Grenzflächen, Center for Integrated Quantum Science and Technology (IQST) and SCoPE, University of Stuttgart, Allmandring 3, 70569 Stuttgart, Germany

[a)]**Author to whom correspondence should be addressed:** jhuebner@nano.uni-hannover.de
[b)]**Electronic mail:** oest@nano.uni-hannover.de

ABSTRACT

We report on the spin and occupation noise of a single, positively charged (InGa)As quantum dot emitting photons in the telecommunication C-band. The spin noise spectroscopy measurements are carried out at a temperature of 4.2 K in dependence on intensity and detuning in the regime beyond thermal equilibrium. The spin noise spectra yield in combination with an elaborate theoretical model the hole-spin relaxation time of the positively charged quantum dot and the Auger recombination and the electron-spin relaxation time of the trion state. The extracted Auger recombination time of this quantum dot emitting at 1.55 μm is comparable to the typical Auger recombination times on the order of a few μs measured in traditionally grown InAs/GaAs quantum dots emitting at around 900 nm.

I. INTRODUCTION

Semiconductor quantum dots (QDs) have attracted significant attention since they are potential solid-state candidates for spin-photon quantum devices[1] and thereby prospective building blocks for future quantum information technologies.[2] Single photon emission from InAs/GaAs QDs at around 900 nm has been established in this context especially during the last decade, but QDs with emission wavelengths at the so-called telecommunication C-band are even more promising from the device point of view. The telecommunication C-band ranges from 1530 to 1565 nm and photons within this band experience an especially low absorption, both within the atmospheric *window* and in optical fibers,[3] promising efficient free-space quantum communication,[4] long-distance fiber communication,[5] and global quantum networks.[6–8]

Ideal quantum dots suitable for spin-photon quantum devices bear long spin relaxation times, negligible charge fluctuations in their surrounding, and low Auger recombination rates. Up to now, InAs/GaAs QDs and more recently strain-free GaAs/AlAs QDs, both with sub-μm wavelength emission, have been optimized in view of these requirements but the respective properties of the relatively new C-band QDs are mainly unexplored so far. In this publication, we show that the method of spin noise spectroscopy (SNS) yields valuable information on all of these three properties also for C-band QDs. This is not trivial since the technology of growing InAs QDs emitting in the telecom C-band is still in its infancy

compared to state-of-the-art QDs emitting in the near-infrared spectral region.

Spin noise spectroscopy optically detects the spin dynamics of atoms and charge carriers via resonant and non-resonant Kerr or Faraday rotation. The technique has been transferred from quantum optics[9,10] to semiconductor physics in 2005[11–14] and applied to single QDs for the first time in 2014.[15] Originally, SNS on single QDs was developed for measuring the undisturbed spin dynamics of single charges. However, Wiegand *et al.*[16] showed that driving the spin system optically beyond the thermal equilibrium allows the concurrent measurement of the complex spin and charge dynamics of a single QD and its local surrounding. At negligible optical excitation, spin noise (SN) of a positively charged QD reveals the intrinsic hole-spin relaxation time only. At finite optical excitation by the SN probe laser, each absorbed photon converts the positively charged exciton into a trion with two holes and one electron. The two holes have in the ground state anti-parallel spins due to the Pauli exclusion principle with a total spin of zero. In that case, the electron spin dominates the spin dynamics of the system. The optically excited trion can either relax via emission of a photon or via Auger recombination. In the latter case, the native hole of the QD is excited out of the QD, the resonance of the QD shifts significantly, and the QD induced Kerr rotation signal at the probe laser wavelength becomes in very good approximation zero, i.e., the spin noise is switched off. This process of switching off the SN is in resonant SNS the typical measure for the Auger recombination rate. At a later time, a hole from the local surrounding tunnels into the unoccupied QD and thereby switches the SN on again, i.e., the SN spectra also contain information on the reloading process.

The measured SNS noise spectra are, therefore, in fact a composite of spin noise (SN) and occupation noise (ON), which both contribute to the noise power spectrum of the QD induced Kerr rotation. The SN and ON contributions can be distinguished easily by (a) the relative detuning of the probe laser light and (b) the magnetic field dependence of the noise power density, which also yields information about the (in)homogeneous QD transition linewidth. Additional measurements of the intensity dependency yield, in turn, information on the Auger coefficient and the influence of power broadening. Thereby, a composite fit of all measured noise spectra in this work yields a more detailed understanding of a typical, state of the art C-band QD.

II. EXPERIMENT

A. Sample

Traditional semiconductor QDs typically emit photons at a wavelength ranging from the visible to the near-infrared. In the past decade, growing InAs QDs on InP substrates has been a common way to shift the emission wavelength further into the infrared region.[7,8,17–24] Such InAs/InP QD systems reach at liquid helium temperatures a ground-state emission wavelength in the telecommunication wavelength regime since the lattice mismatch of InAs/InP is low compared to InAs/GaAs, thus enabling larger QDs with a lower quantization energy. However, the InAs/InP system bears some important limitations like, e.g., the lack of enhanced photon management by distributed Bragg reflector cavities and more challenging mechanical properties compared to the InAs/GaAs systems. Therefore, growing InAs QDs on an (InGa)As metamorphic buffer layer is a promising way to achieve high-quality QDs with emission wavelengths in the telecommunication C-band.[25–32]

The sample studied in this work is such an InAs/GaAs QDs system with a high photon emission yield at around 1550 nm.[28] Figure 1 shows the sample schematically. A 200 nm GaAs buffer is grown on a (100)-oriented GaAs substrate by metal-organic chemical vapor phase epitaxy (MOVPE) in order to achieve a high-quality epitaxial surface. A subsequent nearly lattice-matched distributed Bragg reflector consisting of 20 AlAs(134.4 nm)/GaAs (114.6 nm) pairs enhances the extraction efficiency of the photons emitted from the QDs. The lattice mismatch between InAs and GaAs is reduced to about 4.8% by lattice relaxation in a 1080 nm thick (InGa)As metamorphic buffer layer with linearly increasing indium content from zero to ≈ 36.7%. The InAs QDs are grown on top of the metamorphic layer and capped by a 220 nm thick (InGa)As capping layer. The structure constitutes a nominal low-Q 3λ cavity with a stop-band width of 100 nm where the QDs are in the anti-node of the electric field.[27,28]

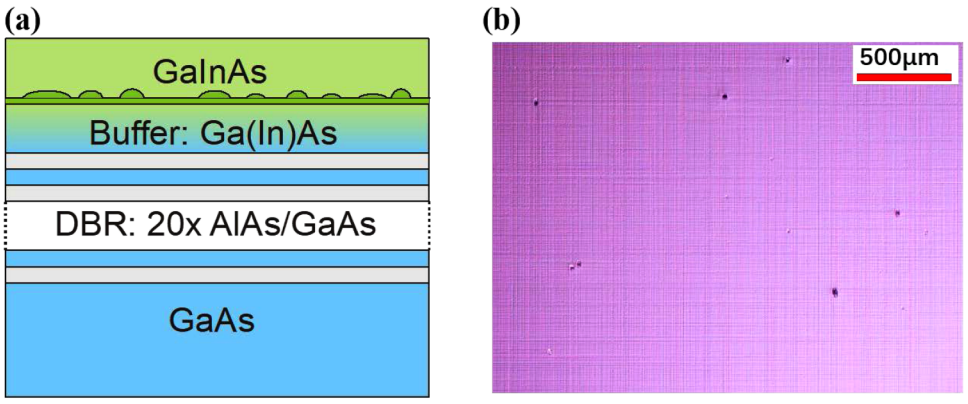

FIG. 1. (a) Schematic structure of the QD sample. (b) The surface of the QD sample shows a cross-hatched pattern with undulations on the μm length scale and a height of a few nm. The distinct points are defects on the surface.

B. Setup

The optical measurements are performed in reflection geometry at cryogenic temperatures. To this end, the sample is mounted in a low-temperature insert in a liquid helium dewar and held at a constant temperature of 4.2 K (see Ref. 15 for details). A 980 nm laser is used for the above bandgap excitation for photoluminescence (PL) characterization. The collected PL signal is dispersed in a high-resolution triple spectrometer and recorded with a liquid nitrogen cooled (InGa)As camera. The MOVPE growth technique inherently incorporates carbon as unintentional background p-type doping into the host material such that a significant part of the QDs are effectively charged at low temperatures by a single hole. The p-type charging type has been shown in a similar sample structure from the same processing batch[33] and agrees as well with the spin noise measurements presented below. The spin and occupation noise measurements are performed with a linearly polarized continuous wave diode laser serving as a probe laser for Kerr rotation measurements in reflection geometry. The laser is focused to a spot of about $3\,\mu$m diameter onto the sample by an aspheric lens with a short focal length. The reflected light containing the Kerr rotation information is analyzed by a balanced photodiode bridge. The electrically amplified signal is Fourier transformed in real-time and averaged. Specially designed superconducting coils provide longitudinal and transverse magnetic fields with a maximum field strength of 31 mT each. The longitudinal magnetic field, which can sufficiently extend the spin relaxation time, is applied when the signal spectrum is recorded and the transverse magnetic field is applied for the background spectrum, which ideally consists of electrical noise and shot noise only. This effectively leaves the measured spin dynamics as a measure of the T_1-time. High-quality, frequency-resolved noise density spectra are obtained by subtracting fore- and background spectra. The noise frequency spectrum in the longitudinal field follows typically a Lorentzian type shape centered at zero frequency. The half-width at half maximum (HWHM) of the Lorentzian is a measure of the correlation rate and the area of the Lorentzian yields the total noise power of the particular contribution. All measurements presented here are carried out in a longitudinal magnetic field of 31 mT, where the influence of the nuclear magnetic field on the carrier spin dynamics is strongly reduced.[15,34] The detuning $\tilde{\Delta}$ of the probe laser light with respect to the maximum of the QD PL spectrum is determined by a wavelength-meter with an accuracy $\ll 1\,\mu$eV. The measured maximum of the PL gives only an estimate of the trion resonance transition energy f_0 since the energy resolution of the PL measurements is limited to $\approx 40\,\mu$eV.

C. Results

Figure 2 shows a typical noise power density spectrum in units of the photon shot noise measured with a probe laser intensity of $8.6\,\mu\mathrm{W}/\mu\mathrm{m}^2$ and a relative detuning of $\Delta = -2.9\,\mu$eV with respect to the trion resonance. This spectrum can be described very well by three Lorentzian contributions with clearly distinguishable HWHM and a common offset. The Kerr rotation noise arises from fluctuations of the electron and hole spins, changes of the QD occupancy, and other noise contributions like, for example, fluctuations of the resonance due to spectral diffusion[32,35] and probably other

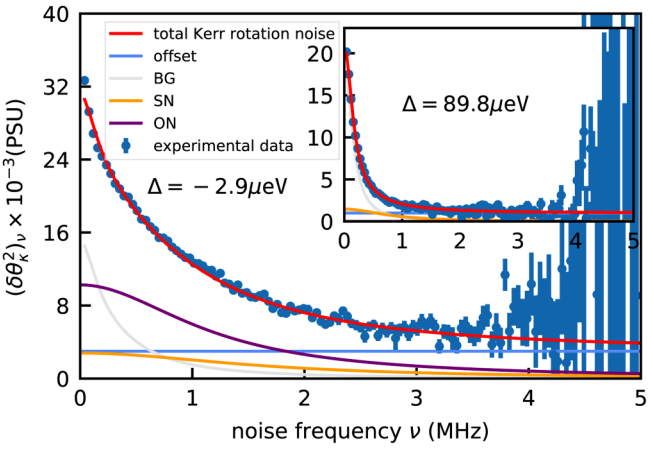

FIG. 2. Typical noise power density spectrum (blue dots) measured at a relatively small laser detuning $\Delta = -2.9\,\mu$eV, i.e., a detuning on the order of the extracted intensity broadened linewidth γ_I. The solid lines are fits according to the theoretical model, which includes the four contributions SN (orange line), ON (magenta line), background (gray line), and offset (light blue line). The red line is the sum of all these contributions. The corresponding fitting parameters and the quantities extracted from the joint fitting of all measurements are summarized in Tables I and II. The inset shows for comparison the spectrum at a large laser detuning of $\Delta = 89.8\,\mu$eV.

QDs in the vicinity of the QD of interest. Two contributions can be easily identified as ON (magenta line) and SN (yellow line) via their different dependency on detuning and probe laser intensity. The ON contribution is dominating close to the trion resonance and at

TABLE I. Parameters of the model for the global fitting. The labels *i*, *f*, *g*, and *gg* denote free in each individual spectrum, fixed, shared within each intensity set, and shared through all spectra, respectively.

Physical quantity	Symbol	Dependency
Offset of Kerr rotation Lorentzian	y0	i
Area of background Lorentzian	A_{bg}	i
Width of background Lorentzian	W_{bg}	i
Area of far-background Lorentzian	A_{fbg}	f
Width of far-background Lorentzian	W_{fbg}	f
Offset of far-background Lorentzian	y_{fbg}	f
Intrinsic transition linewidth	γ	f
Scaling for background-offset	δ	g
Quadratic constant of noise power vs intensity	β	gg
Ratio between γ_A and I_s	α	gg
Trion resonance	f_0	gg
Auger recombination rate	γ_A	gg
Offset of spin relaxation rate profile	$\gamma_{r,\mathrm{sn}}$	gg
Ratio of Auger rate and electron-spin relaxation rate	η	gg
Ratio of P_{on} and P_{sn}	ζ	gg

high laser intensities, i.e., in the case of strong optical excitation. In contrast, the SN contribution is dominating at large detunings where optical excitation becomes weaker and the ON contribution negligible. The exact dependency of these two contributions is extracted from an overall global fitting of the model introduced by Wiegand *et al.*[16,36] to the detuning and intensity-dependent measurements. The model is summarized below in Sec. III.

For the data exemplarily shown in Fig. 2, the HWHM of the SN contribution yields a spin relaxation time of 0.097(2) μs, which is much faster than a typical hole-spin relaxation time.[15,36–38] The reason for this fast spin relaxation is the finite probability for the excitation of the trion under close-to resonance conditions. The optical driving of the transitions results in a *dressed state* representing a coherent superposition of the hole in the ground state and the trion in the excited state. The *dressed state* has a spin relaxation rate, which is a combination of the typically slower hole and faster electron-spin relaxation rate. When the probe laser photon energy is tuned away from the trion resonance, mainly spin fluctuations contribute to the noise frequency spectrum and the ON quickly decreases. For detunings much larger than the optical linewidth, only background noise contributions remain (see the inset of Fig. 2), which origin is not fully clarified yet.

Figure 3 shows the complete detuning dependence for the integrated noise power and the HWHM of the noise frequency spectrum as a function of laser detuning[39] $\tilde{\Delta}$ for SN and ON for a probe laser intensity of 8.6 μW/μm^2. The lines correspond to the model described in Ref. 16 and calculated with the parameters in Table II. The blue dots represent the numerically integrated area of each noise frequency spectrum after subtracting background and offset contributions (gray and blue lines in Fig. 2). The integration is performed up to a cut-off frequency given by the measurement bandwidth Δ^{m}_{BW} (see Fig. 4); hence, the obtained values have to be re-normalized if the width of the dominating contribution exceeds this limit for a correct comparison of fit results and measured data. For the data shown in Fig. 3, the scaling factor is simply obtained by $1/\arctan(\Delta^{m}_{BW}/\max(W_{ON}, W_{SN})$ [for $W_{SN,\,ON}$, see Eq. (10a)].

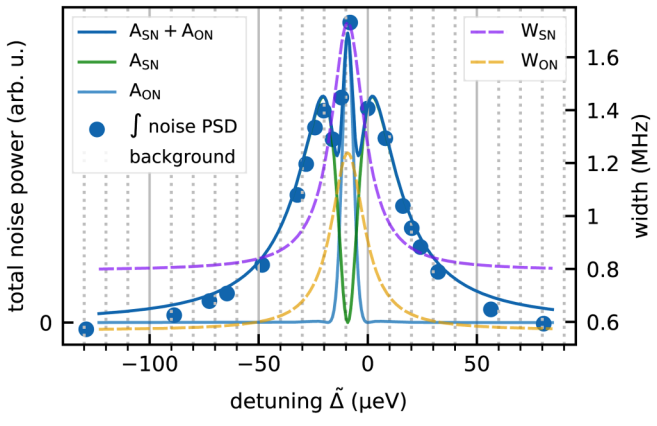

FIG. 3. Integrated noise power and correlation rate as a function of laser detuning at a probe laser intensity of 8.6 μW/μm^2 with respect to the relative probe laser photon energy[39] $\tilde{\Delta}$. The lines show the calculated models with parameters according to Table II. The total integrated noise power (dark blue line) consists of the two contributions of the spin noise (light blue line) and occupation noise power (green line). Shown with respect to the right axis are the correlation rates of spin noise (dashed magenta line) and occupation noise (yellow dash line), respectively. The blue dots denote the cut-off integration of the respective measured noise frequency spectrum. The gray area denotes the magnitude of the background area contribution.

TABLE II. Quantities extracted from the overall global fitting. The specified uncertainties are extracted from the least-square minimization procedure. Further uncertainties might arise from the finite sample quality which is not reproduced by the model.

Physical quantity	Symbol	Value
Trion resonance	f_0	−9.17(8) μeV
Saturation intensity of optical transition	I_s	0.28(1) μW/μm^2
Auger recombination rate	γ_A	1.49(4) MHz
Reoccupation rate	γ_r	0.57(2) MHz
Intrinsic hole-spin relaxation rate[a] (upper limit)	$\gamma_{r,sn}$	0.79(1) MHz
Electron-spin relaxation rate[a]	γ_e	1.94(8) MHz

[a]For $B_z = 31$ mT.

For homogeneously broadened QDs, the detuning dependency of integrated SN power has a *butterfly* shape with two symmetrical maxima located around the QD resonance, whereas the ON power spectrum has a Lorentzian squared-like shape with a single maximum at the QD resonance (see Sec. III). The integrated noise power depicted in Fig. 3 by the solid, dark blue line is the sum of these two contributions. The figure demonstrates that not only the noise power density spectra (Fig. 2) but also the integrated noise power vs detuning is well described by the theoretical model.

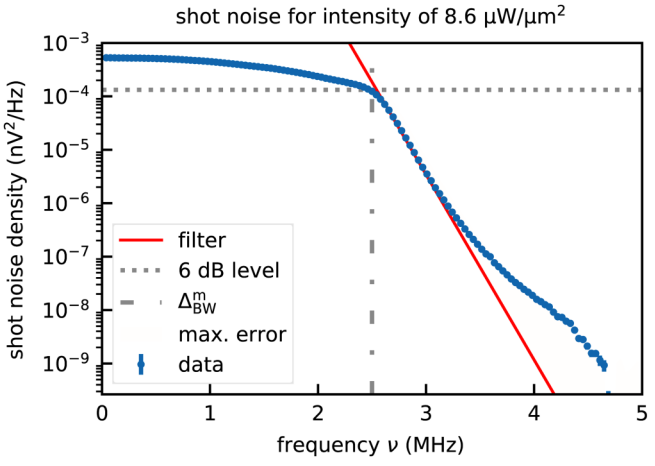

FIG. 4. Measured shot noise spectrum for a given laser intensity (blue dots with error bars). The red line is a fit to an exponential function starting at the data corresponding to the 6 dB point. The light red shaded area is an estimated upper limit of the uncertainty.

The dashed lines in Fig. 3 depict the detuning dependence of the HWHM of the noise power density spectra, i.e., the SN and ON correlation rates, which correspond to the *dressed* spin relaxation rate and occupation rate, respectively. Both rates have a maximum at the QD resonance where the optical absorption has a maximum. For increasing detunings, the dressed trion spin relaxation rate becomes the pure hole spin relaxation rate. Figure 3 also shows that the SN correlation rate is always larger than the ON correlation rate. This is reasonable since a change in QD occupation automatically destroys the QD spin memory.

III. MODEL

In the single positively charged QD, the optical transition between the QD ground and excited states can be described by a four-level system.[40] The ground state is a heavy hole-spin state $|\pm 3/2\rangle$ and the excited state is the trion state, which combines two heavy holes and a single electron spin $|\pm 1/2\rangle$. In the presence of a longitudinal magnetic field, the levels are subjected to a Zeeman splitting $\hbar\Omega_z^h$ and $\hbar\Omega_z^e$ of the ground and excited spin state, respectively. Thus, a linear polarized probe laser can evoke a transition between the ground and excited state based upon the optical selection rules. In the ground state, the heavy hole spin projected along the growth axis contributes to the Kerr rotation. Thus, the spin relaxation rate given by the corresponding HWHM of the Lorentzian-like contributions can be attributed to the heavy hole. In the excited state, the two heavy holes have a total spin projection of zero, thus here the single electron-spin dynamics in the trion dominates the Kerr rotation. In this case, the spin relaxation rate—given by the corresponding HWHM of the Lorentzian-like contribution—is the correlation rate of the trion. Moreover, the Auger process occurs in the trion state, where the resident hole is excited by non-radiative recombination into the valence band with the rate γ_A. The Kerr signal decreases in this case in very good approximation to zero since the resonance shifts significantly when the QD is emptied until a random hole from the surrounding (outer state) re-occupies the QD with the re-occupation rate γ_r. This change between charged and empty QD directly reflects in the Kerr rotation angle and gives rise to occupation noise. In total, spin flips, trion generation, Auger recombination, and QD reoccupation contribute to the noise spectrum at which the generation of the trion state is strongly related to laser intensity and laser detuning. Therefore, the measurement of the detuning dependency and intensity dependency is used to characterize the spin and charge dynamic in the QD.

In the following, we give a compressed overview of all entities entering the evaluation of the data. A full detailed derivation can be found in the former work of Wiegand *et al.*[36] In general, the contributions to the Kerr rotation noise due to spin noise and the QD occupancy fluctuations are given by

$$(\delta\theta_K^2)_{\mathrm{SN}} \sim \left(\frac{2\mathscr{E}\Delta}{\gamma_I^2+\Delta^2}\right)^2 \langle \delta S_z^2\rangle_o, \tag{1a}$$

$$(\delta\theta_K^2)_{\mathrm{ON}} \sim \frac{\mathscr{E}^2(\gamma_I^2-\Delta^2)^2}{4(\gamma_I^2+\Delta^2)^4}\Omega_z^2\langle \delta n^2\rangle_o, \tag{1b}$$

where $\mathscr{E}$ is the effective trion optical transition matrix element, which can be related to the probe laser intensity and Δ is the detuning with respect to the trion resonance. The total spin S_z projected along the growth and optical detection axis is given by

$$\langle \delta S_z^2\rangle_o = \frac{\overline{n}}{4}, \tag{2}$$

where $\overline{n}$ is the average QD occupancy, which is determined by the generation rate G, the trion recombination rate R, the Auger recombination rate γ_A, and the QD reoccupation rate γ_r [cf. Eq. (S25) of Ref. 36],

$$\overline{n} = \frac{\gamma_r(G+R)}{\gamma_r(G+R)+\gamma_A G}. \tag{3}$$

The QD occupancy fluctuations are then obtained via

$$\langle \delta n^2\rangle_o = \overline{n}(1-\overline{n}). \tag{4}$$

Finally, the integrated noise power spectra of SN and ON, respectively, are given by

$$(\delta\theta_K^2)_{\mathrm{SN}} = \frac{2P_{\mathrm{sn}}\Delta^2}{(\gamma_I^2+\Delta^2)(\gamma_2^2+\Delta^2)}, \tag{5a}$$

$$(\delta\theta_K^2)_{\mathrm{ON}} = \frac{P_{\mathrm{on}}(\gamma_2^2-\gamma_I^2)(\gamma_I^2-\Delta^2)^2}{4(\gamma_I^2+\Delta^2)^3(\gamma_2^2+\Delta^2)^2}. \tag{5b}$$

The magnitude of the measured spin noise power spectrum P_{sn} is proportional to the quadratic probe laser power, which can be replaced by the intensity I in this case since the excitation area is fixed for all measurements (the unit conversion is absorbed in the constant β),

$$P_{\mathrm{sn}} = \beta \cdot I^2. \tag{6}$$

The ratio between $P_{\mathrm{on}}/P_{\mathrm{sn}} = \zeta$ enters as a fitting parameter, which includes the occupation probability of the quantum dot as well as the Larmor frequency Ω_z corresponding to the effective trion Zeeman splitting in z-direction, which, however, cannot be unambiguously determined from the available data within the current evaluation. The trion linewidth γ_I due to saturation broadening[16,41] depends on the probe laser intensity as

$$\gamma_I = \gamma\sqrt{1+2\frac{\mathscr{E}^2}{\gamma\gamma_0}} = \gamma\sqrt{1+\frac{I}{I_s}}, \tag{7}$$

where I_s is the saturation intensity, γ_0 is the spontaneous recombination rate, and γ the intrinsic transition linewidth, which is taken as $1.65 \pm 0.87\,\mu$eV from the resonance fluorescence measurements in Table 1 of Ref. 42. The latter three quantities are interrelated by

$$\frac{\mathscr{E}^2}{\gamma_0} = \frac{I\gamma}{2I_s}. \tag{8}$$

Due to Auger recombination, occupation noise is much more prominent at smaller detunings while spin noise is more dominant at larger detunings. Hence, the trion transition width—denoted by γ_2—is additionally broadened beyond γ_I resulting from Auger recombination,

$$\gamma_2^2 = \gamma_I^2 + \frac{\gamma_A \gamma \mathscr{E}^2}{\gamma_r \gamma_0} = \gamma_I^2 + \frac{\gamma_A \gamma^2 I}{2 I_s \gamma_r}. \tag{9}$$

Here again, γ_r is the re-occupation rate, which can be estimated from the offset of the occupation rate profile (yellow dashed line in Fig. 3). The spin relaxation rate and occupation rate profiles are described by the two Lorentzians,

$$W_{\mathrm{SN}} = A_{\mathrm{SN}} \frac{\gamma_I}{\pi(\gamma_1^2 + \Delta^2)} + \gamma_{r,\mathrm{sn}}, \tag{10a}$$

$$W_{\mathrm{ON}} = A_{\mathrm{ON}} \frac{\gamma_I}{\pi(\gamma_1^2 + \Delta^2)} + \gamma_{r,\mathrm{on}}. \tag{10b}$$

Here, the offset $\gamma_{r,\mathrm{sn}}$ corresponds to the intrinsic spin relaxation rate, whereas $\gamma_{r,\mathrm{on}}$ corresponds to the re-occupation rate γ_r of the QD. Both profiles share the same trion HWHM linewidth γ_I.

The area of the spin noise width profile A_{SN} and the area of occupation noise width profile A_{ON} are given by

$$A_{\mathrm{SN}} = \frac{\pi}{2} \frac{I\gamma}{\sqrt{I_s(I + I_s)}} \gamma_e, \tag{11a}$$

$$A_{\mathrm{ON}} = \frac{\pi}{2} \frac{I\gamma}{\sqrt{I_s(I + I_s)}} \gamma_A, \tag{11b}$$

where γ_e is the electron-spin relaxation rate. In order to avoid non-physical solutions, we constrain the ratio between occupation noise width and spin noise width by

$$\frac{\gamma_{r,\mathrm{sn}}}{\gamma_{r,\mathrm{on}}} = \eta \geqslant 1 \quad \text{and} \quad \frac{\gamma_e}{\gamma_A} = \eta \geqslant 1. \tag{12}$$

In the overall global fitting procedure, each noise power density spectrum $\langle \delta\theta_{\mathrm{K}}^2 \rangle$ consists of a SN Lorentzian L_{SN}, an ON Lorentzian L_{ON}, a background contribution L'_{BG}, and an offset y_0. For example, the SN Lorentzian describing the corresponding noise power density spectrum reads as a function of the noise frequency ν,

$$L_{\mathrm{SN}}\langle \nu \rangle = \frac{(\delta\theta_K^2)_{\mathrm{SN}}}{\pi} \frac{W_{\mathrm{SN}}}{W_{\mathrm{SN}}^2 + \nu^2}, \tag{13}$$

where the respective noise power $(\delta\theta_K^2)_{\mathrm{SN}}$ is defined in Eq. (5a). The contribution L'_{BG} is split into an independent and a fixed part determined at the largest detunings, whereas the fixed part possibly arises from contributions from remote QDs. The detuning-dependent background is depicted as gray area in Fig. 3. The constant offset is attributed to a difference in the shot noise level between the subsequently recorded fore- and background spectra at different applied magnetic fields.

Finally, the above model yields all the parameters needed for the overall global fitting, as shown in Table I. In the fitting procedure, parameters labeled with i are set to free through all noise frequency spectra, parameters labeled with f are fixed, parameters labeled with g are shared within each intensity set, and parameters labeled with gg are shared through all spectra. Naturally, all parameters directly related to the QD are shared through all spectra since the QD itself does not change during the measurement.

IV. DISCUSSION

Table II shows all extracted physical quantities related to the optical transition, the electron and hole spin, and the charge dynamics. The quantities are extracted from the overall global fitting of all measured spectra via a standard least-square minimization. The overall global fitting reveals an Auger recombination time of $0.72(2)\,\mu$s and a re-occupation time of $1.76(5)\,\mu$s, which are comparable to measurements on traditional single self-assembled QDs emitting at ≈ 900 nm.[36,43] The long re-occupation time suggests a slow recapturing process from the outer states, indicating a low p-type carbon background doping density. Regarding the spin dynamics, we obtain a T_1 electron-spin relaxation time at $B_{\mathrm{ext}} = 31$ mT of $0.52(2)\,\mu$s and a hole-spin relaxation time of $1.26(2)\,\mu$s, which is two orders of magnitude faster than previous measurements of the hole-spin relaxation time with one order of magnitude lower probe intensity in higher lattice mismatch QDs.[15] Such a short hole-spin lifetime is surely limited by the non-equilibrium environment driven by higher probe intensity and also limited by the remaining hyperfine interaction due to the presence of the nuclei spin bath, which is only suppressed to some extend by the longitudinal magnetic field.[44] Nevertheless, the hole-spin relaxation time is longer than the electron-spin relaxation time since the electron-spin relaxation is usually more strongly influenced by hyperfine interaction than the hole-spin relaxation.[35]

Many measurements of quantum dots show electron-spin relaxation times of a few ns due to a finite nuclear magnetic field.[38,45,46] The longer electron-spin relaxation obtained here suggests that the nuclear hyperfine interaction with the electron is efficiently suppressed by the external magnetic field. The overall global fitting also yields a transition linewidth which amounts, e.g., for the case of a probe laser intensity of $8.6\,\mu\mathrm{W}/\mu\mathrm{m}^2$ to approximately $9.2 \pm 4.8\,\mu$eV. The smaller value of the intrinsic linewidth γ demonstrates that the measurements are taken in a regime dominated by saturation broadening, which is also reflected by the extracted low saturation intensity $I_s = 0.28(1)\,\mu\mathrm{W}/\mu\mathrm{m}^2$.

V. CONCLUSION

We have measured spin noise and occupation noise under non-equilibrium conditions for the first time in a single, positively charged (InGa)As QD with a photon emission energy at telecommunication wavelengths. The full analysis of intensity-dependent measurements reveals the trion spin dynamics under resonant and nearly resonant excitation conditions. We extract both the electron- and the hole-spin lifetime from the spin noise contribution and the

Auger recombination rate and the reoccupation rate from the occupation noise contribution. The analysis yields additionally the saturation intensity of the optical QD transition, the effective trion Zeeman splitting, and allows inferring on the impact of the QD surrounding. In this experiment, the optical quality of the QD was not yet optimized and the noise spectra showed contributions from QDs in the direct spatial surrounding. Well separated QDs with higher optical quality will show less background contributions, simplifying the evaluation of the noise spectra enormously. In that case, spin noise spectroscopy becomes an excellent characterization tool for C-band QDs having a significant impact on the development of these QDs and their applicability in future quantum communication.

ACKNOWLEDGMENTS

We acknowledge financial support by the Deutsche Forschungsgemeinschaft (DFG, German Research Foundation) under Germany's Excellence Strategy—EXC-2123 QuantumFrontiers—390837967, and OE 177/10-2. T.-J.S. acknowledges financial support by the China Scholarship Council (CSC). C.N., M.J., and P.M. gratefully acknowledge the funding by the German Federal Ministry of Education and Research (BMBF) via the Project QR.X (No. 16KISQ013).

AUTHOR DECLARATIONS

Conflict of Interest

The authors declare that they have no conflicts of interest.

APPENDIX: DATA ANALYSIS

1. Measurement bandwidth

Measuring a frequency power density spectrum often bears some easy-to-follow but nevertheless important points. One of them concerns the typically limited measurement bandwidth $\Delta^{\mathrm{m}}_{\mathrm{BW}}$ of the detection path in conjunction with the sampling frequency f_{s} of the data acquisition equipment. As a rule of thumb the Nyquist–Shannon theorem demands $f_{\mathrm{s}} \geq 2 \cdot \Delta^{\mathrm{m}}_{\mathrm{BW}}$ at least for bandwidths starting at zero frequency. If this condition cannot be fulfilled in the first place, typically cut-off filters ensure that the measured data do not contain signals arising from the so-called under-sampling effect. For the data presented in this work, the Nyquist–Shannon condition is well satisfied for the detection bandwidth of the balanced receiver of $\Delta^{\mathrm{m}}_{\mathrm{BW}} \approx 2.5\,\mathrm{MHz}$ by the sampling frequency of $f_{\mathrm{s}} = 10\,\mathrm{MHz}$. However, the finite bandwidth entails of course that the shape of the measured spectra exceeding $\Delta^{\mathrm{m}}_{\mathrm{BW}}$ is distorted by the decrease in the effective measurement sensitivity. The typical procedure is to normalize the measured spectra by the sensitivity, or equivalently, as in our case, by the measured optical shot noise. Figure 4 exemplarily shows the measured optical shot noise power density with the strong drop in sensitivity beyond the 6 dB point of the optical filter. The red line is an exponential approximation of the filter characteristics. The noise floor is dominated for frequencies beyond ≈4 MHz by the noise from the electronic amplifiers in the data acquisition path. The measured raw Faraday fluctuation spectra show of course the same characteristics.

2. Shot noise normalization

Potentially very large systematic deviations can emerge if the signal is normalized to a shot noise spectrum, which includes very small values like in Fig. 4. The difficulty arises, for example, if the spectrum contains an offset which is determined with very high precision but poor accuracy. In this case, even the incredible small values at $\nu > \Delta^{\mathrm{m}}_{\mathrm{BW}}$ evoke a non-negligible biased impact on the fitting procedure—even if a correct uncertainty propagation is followed. An easy solution would be to restrain all evaluations to a fixed limit, e.g., the 6 dB point of the detector. However, most detectors have a usable dynamic range of at least 20 dB. In order to systematically harness all measured data points, an upper limit of the systematic uncertainties could be estimated from the filter characteristics which can enter—if needed—via error propagation the measured data. This procedure could potentially ensure a reliable filtering of the data, however, at the price of an artificially deformed statistics of the residuals, i.e., quite a number of very small residuals would appear as a narrow peak in the distribution of the residuals.

In the data presented here, all spectra are normalized to the respective measured shot noise spectra (blue dots in Fig. 4). However, we assume that the foreground and background spectra have in theory exactly the same noise level at 5 MHz and realign the background spectra accordingly by a constant offset. This offset is lower than a factor of 10^{-4} of the original signal throughout all spectra. The result of this procedure can be seen exemplarily in the data and their corresponding uncertainties shown in Fig. 2. This approach is rewarded by a well distributed residual statistic for the final fit result (see Fig. 5).

3. Data binning (resampling)

The original spectra have been recorded with a much higher resolution than shown in Fig. 2. The spectra have been binned to a

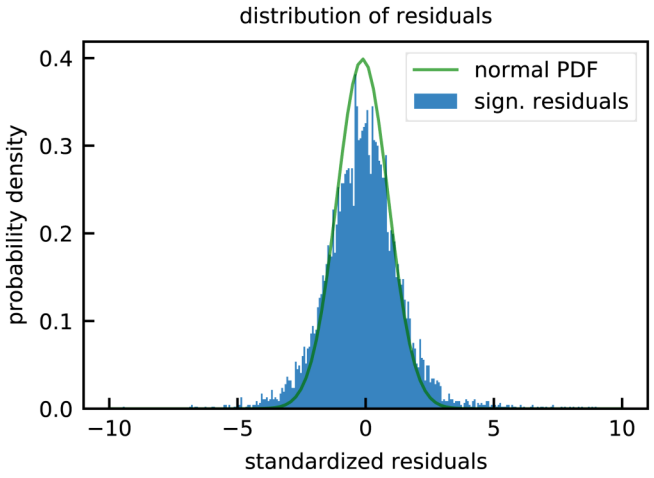

FIG. 5. Distribution of standardized residuals of the SN model fitted to the data (blue). The green line follows a Gaussian normal distribution.

lower resolution in order to ease the numerical evaluation without significantly affecting the extracted quantities.

4. Model statistics

In order to judge how well the complete model describes the measured data, we perform a short statistical analysis. Figure 5 displays the distribution of the standardized residuals of the fitted model. The distributions contain all residuals e_{res} and give a standard deviation of $\chi^2 = 2.76$, which is admittedly larger than the ideal unity but not too far off. A value of $\chi^2 > 1$ suggests that either the uncertainties of the data points are underestimated or that the model is not that suitable. However, in the latter case, there would typically appear a skewness in the distribution, which is not the case here.

DATA AVAILABILITY

The data that support the findings of this study are available from the corresponding author upon reasonable request.

REFERENCES

[1]C. Arnold, J. Demory, V. Loo, A. Lemaître, I. Sagnes, M. Glazov, O. Krebs, P. Voisin, P. Senellart, and L. Lanco, "Macroscopic rotation of photon polarization induced by a single spin," Nat. Commun. **6**, 153 (2015).

[2]K. De Greve, L. Yu, P. L. McMahon, J. S. Pelc, C. M. Natarajan, N. Y. Kim, E. Abe, S. Maier, C. Schneider, M. Kamp, S. Höfling, R. H. Hadfield, A. Forchel, M. M. Fejer, and Y. Yamamoto, "Quantum-dot spin-photon entanglement via frequency downconversion to telecom wavelength," Nature **491**, 421–425 (2012).

[3]S. L. Portalupi, M. Jetter, and P. Michler, "InAs quantum dots grown on metamorphic buffers as non-classical light sources at telecom C-band: A review," Semicond. Sci. Technol. **34**, 053001 (2019).

[4]S.-K. Liao, H.-L. Yong, C. Liu, G.-L. Shentu, D.-D. Li, J. Lin, H. Dai, S.-Q. Zhao, B. Li, J.-Y. Guan, W. Chen, Y.-H. Gong, Y. Li, Z.-H. Lin, G.-S. Pan, J. S. Pelc, M. M. Fejer, W.-Z. Zhang, W.-Y. Liu, J. Yin, J.-G. Ren, X.-B. Wang, Q. Zhang, C.-Z. Peng, and J.-W. Pan, "Long-distance free-space quantum key distribution in daylight towards inter-satellite communication," Nat. Photonics **11**, 509–513 (2017).

[5]G. P. Agrawal, *Fiber-Optic Communication Systems* (John Wiley & Sons, 2010).

[6]K. Takemoto, M. Takatsu, S. Hirose, N. Yokoyama, Y. Sakuma, T. Usuki, T. Miyazawa, and Y. Arakawa, "An optical horn structure for single-photon source using quantum dots at telecommunication wavelength," J. Appl. Phys. **101**, 081720 (2007).

[7]J.-H. Kim, T. Cai, C. J. K. Richardson, R. P. Leavitt, and E. Waks, "Two-photon interference from a bright single-photon source at telecom wavelengths," Optica **3**, 577–584 (2016).

[8]M. Anderson, T. Müller, J. Huwer, J. Skiba-Szymanska, A. B. Krysa, R. M. Stevenson, J. Heffernan, D. A. Ritchie, and A. J. Shields, "Quantum teleportation using highly coherent emission from telecom C-band quantum dots," npj Quantum Inf. **6**, 14 (2020).

[9]E. B. Aleksandrov and V. S. Zapasskil, "Magnetic resonance in the Faraday-rotation noise spectrum," Zh. Eksp. Teor. Fiz. **81**, 132–138 (1981) [Sov. Phys. JETP **54**, 64 (1981)].

[10]S. A. Crooker, D. G. Rickel, A. V. Balatsky, and D. L. Smith, "Spectroscopy of spontaneous spin noise as a probe of spin dynamics and magnetic resonance," Nature **431**, 49–52 (2004).

[11]M. Oestreich, M. Römer, R. J. Haug, and D. Hägele, "Spin noise spectroscopy in GaAs," Phys. Rev. Lett. **95**, 216603 (2005).

[12]M. Römer, J. Hübner, and M. Oestreich, "Spin noise spectroscopy in semiconductors," Rev. Sci. Instrum. **78**, 103903 (2007).

[13]G. M. Müller, M. Oestreich, M. Römer, and J. Hübner, "Semiconductor spin noise spectroscopy: Fundamentals, accomplishments, and challenges," Physica E **43**, 569–587 (2010).

[14]V. S. Zapasskii, "Spin-noise spectroscopy: From proof of principle to applications," Adv. Opt. Photonics **5**, 131–168 (2013).

[15]R. Dahbashi, J. Hübner, F. Berski, K. Pierz, and M. Oestreich, "Optical spin noise of a single hole spin localized in an (InGa)As quantum dot," Phys. Rev. Lett. **112**, 156601 (2014).

[16]J. S. Wiegand, "Nonequilibrium spin noise spectroscopy on single quantum dots," Ph.D. thesis (Institutionelles Repositorium der Leibniz Universität Hannover, Hannover, 2019).

[17]T. Miyazawa, K. Takemoto, Y. Sakuma, S. Hirose, T. Usuki, N. Yokoyama, M. Takatsu, and Y. Arakawa, "Single-photon generation in the 1.55-μm optical-fiber band from an InAs/InP quantum dot," Jpn. J. Appl. Phys. **44**, L620 (2005).

[18]R. Nötzel, S. Anantathanasarn, R. P. J. V. Veldhoven, F. W. M. V. Otten, T. J. Eijkemans, A. Trampert, B. Satpati, Y. Barbarin, E. A. J. M. Bente, Y.-S. Oei, T. D. Vries, E.-J. Geluk, B. Smalbrugge, M. K. Smit, and J. H. Wolter, "Self-assembled InAs/InP quantum dots for telecom applications in the 1.55 μm wavelength range: Wavelength tuning, stacking, polarization control, and lasing," Jpn. J. Appl. Phys. **45**, 6544 (2006).

[19]M. D. Birowosuto, H. Sumikura, S. Matsuo, H. Taniyama, P. J. van Veldhoven, R. Nötzel, and M. Notomi, "Fast Purcell-enhanced single photon source in 1550-nm telecom band from a resonant quantum dot-cavity coupling," Sci. Rep. **2**, 321 (2012).

[20]M. Benyoucef, M. Yacob, J. P. Reithmaier, J. Kettler, and P. Michler, "Telecom-wavelength (1.5 μm) single-photon emission from InP-based quantum dots," Appl. Phys. Lett. **103**, 162101 (2013).

[21]X. Liu, K. Akahane, N. A. Jahan, N. Kobayashi, M. Sasaki, H. Kumano, and I. Suemune, "Single-photon emission in telecommunication band from an InAs quantum dot grown on InP with molecular-beam epitaxy," Appl. Phys. Lett. **103**, 061114 (2013).

[22]Ł. Dusanowski, M. Syperek, P. Mrowiński, W. Rudno-Rudziński, J. Misiewicz, A. Somers, S. Höfling, M. Kamp, J. P. Reithmaier, and G. Sęk, "Single photon emission at 1.55 μm from charged and neutral exciton confined in a single quantum dash," Appl. Phys. Lett. **105**, 021909 (2014).

[23]A. Kors, K. Fuchs, M. Yacob, J. P. Reithmaier, and M. Benyoucef, "Telecom wavelength emitting single quantum dots coupled to InP-based photonic crystal microcavities," Appl. Phys. Lett. **110**, 031101 (2017).

[24]T. Müller, J. Skiba-Szymanska, A. B. Krysa, J. Huwer, M. Felle, M. Anderson, R. M. Stevenson, J. Heffernan, D. A. Ritchie, and A. J. Shields, "A quantum light-emitting diode for the standard telecom window around 1550 nm," Nat. Commun. **9**, 862 (2018).

[25]E. S. Semenova, R. Hostein, G. Patriarche, O. Mauguin, L. Largeau, I. Robert-Philip, A. Beveratos, and A. Lemaître, "Metamorphic approach to single quantum dot emission at 1.55 μm on GaAs substrate," J. Appl. Phys. **103**, 103533 (2008).

[26]L. Seravalli, G. Trevisi, P. Frigeri, D. Rivas, G. Muñoz-Matutano, I. Suárez, B. Alén, J. Canet-Ferrer, and J. P. Martínez-Pastor, "Single quantum dot emission at telecom wavelengths from metamorphic InAs/InGaAs nanostructures grown on GaAs substrates," Appl. Phys. Lett. **98**, 173112 (2011).

[27]F. Olbrich, J. Höschele, M. Müller, J. Kettler, S. Luca Portalupi, M. Paul, M. Jetter, and P. Michler, "Polarization-entangled photons from an InGaAs-based quantum dot emitting in the telecom C-band," Appl. Phys. Lett. **111**, 133106 (2017).

[28]M. Paul, F. Olbrich, J. Höschele, S. Schreier, J. Kettler, S. L. Portalupi, M. Jetter, and P. Michler, "Single-photon emission at 1.55 μm from MOVPE-grown InAs quantum dots on InGaAs/GaAs metamorphic buffers," Appl. Phys. Lett. **111**, 033102 (2017).

[29]X. Cao, M. Zopf, and F. Ding, "Telecom wavelength single photon sources," J. Semicond. **40**, 071901 (2019).

[30]Ł. Dusanowski, C. Nawrath, S. L. Portalupi, M. Jetter, T. Huber, S. Klembt, P. Michler, and S. Höfling, "Optical charge injection and full coherent control of spin-qubit in the telecom C-band emitting quantum dot," arXiv:2107.06367 [cond-mat.mes-hall] (2021).

[31]K. D. Zeuner, K. D. Jöns, L. Schweickert, C. Reuterskiöld Hedlund, C. Nuñez Lobato, T. Lettner, K. Wang, S. Gyger, E. Schöll, S. Steinhauer, M. Hammar, and V. Zwiller, "On-demand generation of entangled photon pairs in the telecom C-band with InAs quantum dots," ACS Photonics **8**, 2337–2344 (2021).
[32]C. Nawrath, H. Vural, J. Fischer, R. Schaber, S. L. Portalupi, M. Jetter, and P. Michler, "Resonance fluorescence of single In(Ga)As quantum dots emitting in the telecom C-band," Appl. Phys. Lett. **118**, 244002 (2021).
[33]C. Carmesin, F. Olbrich, T. Mehrtens, M. Florian, S. Michael, S. Schreier, C. Nawrath, M. Paul, J. Höschele, B. Gerken, J. Kettler, S. L. Portalupi, M. Jetter, P. Michler, A. Rosenauer, and F. Jahnke, "Structural and optical properties of InAs/(In)GaAs/GaAs quantum dots with single-photon emission in the telecom C-band up to 77 K," Phys. Rev. B **98**, 125407 (2018).
[34]B. D. Gerardot, D. Brunner, P. A. Dalgarno, P. Öhberg, S. Seidl, M. Kroner, K. Karrai, N. G. Stoltz, P. M. Petroff, and R. J. Warburton, "Optical pumping of a single hole spin in a quantum dot," Nature **451**, 441–444 (2008).
[35]R. J. Warburton, "Single spins in self-assembled quantum dots," Nat. Mater. **12**, 483 (2013).
[36]J. Wiegand, D. S. Smirnov, J. Hübner, M. M. Glazov, and M. Oestreich, "Spin and reoccupation noise in a single quantum dot beyond the fluctuation-dissipation theorem," Phys. Rev. B **97**, 081403 (2018).
[37]Y. Li, N. Sinitsyn, D. L. Smith, D. Reuter, A. D. Wieck, D. R. Yakovlev, M. Bayer, and S. A. Crooker, "Intrinsic spin fluctuations reveal the dynamical response function of holes coupled to nuclear spin baths in (In, Ga)As quantum dots," Phys. Rev. Lett. **108**, 186603 (2012).
[38]P. Glasenapp, D. S. Smirnov, A. Greilich, J. Hackmann, M. M. Glazov, F. B. Anders, and M. Bayer, "Spin noise of electrons and holes in (In,Ga)As quantum dots: Experiment and theory," Phys. Rev. B **93**, 205429 (2016).
[39]The detuning with respect to the trion resonance f_0 is labeled as Δ, whereas $\tilde{\Delta} = \Delta + f_0$ is the probe laser photon energy measured relative to the wave-meter.
[40]D. S. Smirnov, P. Glasenapp, M. Bergen, M. M. Glazov, D. Reuter, A. D. Wieck, M. Bayer, and A. Greilich, "Nonequilibrium spin noise in a quantum dot ensemble," Phys. Rev. B **95**, 241408 (2017).
[41]W. Demtröder, *Laserspektroskopie: Grundlagen und Techniken* (Springer-Verlag, 2007).
[42]C. Nawrath, F. Olbrich, M. Paul, S. L. Portalupi, M. Jetter, and P. Michler, "Coherence and indistinguishability of highly pure single photons from non-resonantly and resonantly excited telecom C-band quantum dots," Appl. Phys. Lett. **115**, 023103 (2019).
[43]A. Kurzmann, A. Ludwig, A. D. Wieck, A. Lorke, and M. Geller, "Auger recombination in self-assembled quantum dots: Quenching and broadening of the charged exciton transition," Nano Lett. **16**, 3367–3372 (2016).
[44]J. H. Prechtel, A. V. Kuhlmann, J. Houel, A. Ludwig, S. R. Valentin, A. D. Wieck, and R. J. Warburton, "Decoupling a hole spin qubit from the nuclear spins," Nat. Mater. **15**, 981–986 (2016).
[45]I. A. Merkulov, A. L. Efros, and M. Rosen, "Electron spin relaxation by nuclei in semiconductor quantum dots," Phys. Rev. B **65**, 205309 (2002).
[46]S. A. Crooker, J. Brandt, C. Sandfort, A. Greilich, D. R. Yakovlev, D. Reuter, A. D. Wieck, and M. Bayer, "Spin noise of electrons and holes in self-assembled quantum dots," Phys. Rev. Lett. **104**, 036601 (2010).